

A new vehicle specific power method based on internally observable variables: Application to CO₂ emission assessment for a hybrid electric vehicle

Wenli Wang^{a,c,1}, Jing Bie^{b,1}, Abubakar Yusuf^a, Yiqiang Liu^c, Xiaofei Wang^c, Chengjun Wang^d, George Zheng Chen^e, Jianrong Li^f, Dongsheng Ji^g, Hang Xiao^f, Yong Sun^a, Jun He^{a,h,*}

^a Department of Chemical and Environmental Engineering, University of Nottingham Ningbo China, Ningbo, China

^b Department of Civil Engineering, University of Nottingham Ningbo China, Ningbo, China

^c Ningbo Geely Royal Engine Components Co. Ltd, Hangzhou Bay New Area, Ningbo, China

^d College of Resources and Environmental Sciences, South-Central Minzu University, Wuhan, China

^e Department of Chemical and Environmental Engineering, Faculty of Engineering, University of Nottingham, UK

^f Center for Excellence in Regional Atmospheric Environment, Institute of Urban Environment, Chinese Academy of Sciences, Xiamen, China

^g State Key Laboratory of Atmospheric Boundary Layer Physics and Atmospheric Chemistry, Institute of Atmospheric Physics, Chinese Academy of Sciences, Beijing, China

^h Nottingham Ningbo China Beacons of Excellence Research and Innovation Institute, Ningbo, China

ARTICLE INFO

Keywords:

Vehicle specific power
Hybrid electric vehicle
CO₂ emission
Real-world driving emission
Hybrid working mode

ABSTRACT

As an important vehicle activity recognition method, vehicle specific power (VSP) has been widely used for on-road traffic emission modelling since its introduction in 1999. The conventional VSP (VSP_{veh}) is calculated from externally observable variables (EOVs) on the vehicle level and represents the power that a running vehicle needs to overcome. However, for hybrid electric vehicles (HEVs) with two power sources, vehicle activity is not always directly related to engine emissions. This study introduces the engine level VSP (VSP_{eng}), which estimates engine power from internally observable variables (IOVs) obtained from the vehicle's on-board electronic control unit (ECU). An engine bench test is first implemented to validate the estimation algorithm for VSP_{eng}. A real-world driving emission (RDE) test is then conducted with a HEV in Ningbo city of China to evaluate the performance of VSP_{veh} and VSP_{eng} in emission estimation. The results show a strong correlation between emission and VSP_{eng} ($R^2 = 0.9783$), while a much weaker correlation was found between emission and VSP_{veh} ($R^2 = 0.4216$). Further analysis indicates that this strong correlation between emission and VSP_{eng} applies to all driving conditions (urban, rural and highway). The differences between VSP_{veh} and VSP_{eng} are then highlighted by a combined correlation analysis where the four work modes of HEV can be graphically identified. Lastly, this study discusses the feasibility and potential benefits of the intelligent and remote vehicle emissions monitoring through the upcoming vehicle to everything (V2X) network.

1. Introduction

Fuel consumption of transport systems is a main contributor to greenhouse gas (GHG) emission and global warming [7,8,9,10,11]. Initiatives are being proposed and undertaken across the globe to reduce

GHG emission and mitigate global warming. The Chinese government is currently promoting carbon neutrality and striving for carbon dioxide emissions to reach a peak by 2030 [24]. Within the passenger vehicle sector, as a modified version of California's Zero Emission Vehicle Mandate, China introduced its latest New-Energy Vehicle (NEV)

Abbreviations: CAN, Controller area network; ECU, Engine control unit; EOVs, Externally observable variables; HEV, Hybrid electric vehicle; IOVs, Internally observable variables; MOVES, Motor vehicle emission simulator; OBD, On-board diagnostic; PEMS, Portable emission measurement system; RDE, Real-world driving emission; VSP, Vehicle specific power; VSP_{eng}, VSP from engine level; VSP_{veh}, VSP from vehicle level.

* Corresponding author at: Department of Chemical and Environmental Engineering, University of Nottingham Ningbo China, Ningbo, China.

E-mail address: jun.he@nottingham.edu.cn (J. He).

¹ These authors equally contributed to this work.

<https://doi.org/10.1016/j.enconman.2023.117050>

Received 5 February 2023; Received in revised form 9 April 2023; Accepted 12 April 2023

Available online 21 April 2023

0196-8904/© 2023 The Author(s). Published by Elsevier Ltd. This is an open access article under the CC BY-NC-ND license (<http://creativecommons.org/licenses/by-nc-nd/4.0/>).

mandate policy in 2020 with specific NEV “credit” requirement for all car-makers, and specified the more stringent stage 5 target for Corporate Average Fuel Consumption (CAFC) to achieve 4 L/100 km in 2025 from 5 L/100 km in 2020 [20,21,22,23]. Driven by these policies, the Chinese automotive market is experiencing a large-scale electrification: many Chinese car-makers have formulated a series of radical transformation plans for NEV, with development projects on Hybrid Electric Vehicles (HEVs) in the short term, and Battery Electrical Vehicles (BEVs) and Fuel Cell Electric Vehicles (FCEVs) in the long term.

The quantitative description of vehicle emissions is an important tool to support decision making in vehicle emission control by identifying detailed characteristics and sources of emissions [3,14]. In US and EU, there are various vehicle emission models for on-road emission estimation, such as the MOTO Vehicle Emission Simulator (MOVES) developed by US Environmental Protection Agency [27,28] and the Computer Program to calculate Emissions from Road Transport (COPERT) developed by the European Commission (JRC) [11]. By considering the characteristics of various vehicle types and real-world emission data collected from the US market over many years, MOVES has been widely used as an estimation tool to quantify vehicle emission. In China, the upcoming national stage 6 (phase b) emission standard for light-duty passenger vehicle will introduce more stringent emission conformity limits for real-world driving emission (RDE) in 2023 [20].

The Vehicle Specific Power (VSP) method developed by José L. Jiménez (1999) links emission to vehicle activity [13,6], and has been adopted by the MOVES model for vehicle emission simulation and database establishment starting from its first version issued in 2010 [28]. Since then, VSP has been extensively applied in many studies as an indicator for engine load in different vehicles and road conditions [4,12,42,30]. However, these VSP models require emission datasets from a large number of tested vehicles under pre-defined drive cycle in chassis dynamometer or drive route on the road. Duarte et al. [5] tested 19 vehicles under on-road conditions in the Lisbon Metropolitan Area, Portugal to establish the relationship between fuel consumption and VSP; Wu et al. [34] employed 22 vehicles to link black carbon emission rates with VSP in China; Park et al. [25] tested 17 light-duty vehicles mainly sold in Korea to develop CO₂ emission rate associated with VSP. It is apparently very expensive and time-consuming to conduct such extensive emission tests for every vehicle model across different regions with Portable Emission Measurement System (PEMS). Zhai et al. [41] raised a very straightforward question “How much vehicle activity data is needed to develop robust VSP distributions for emission estimates?” and attempted to answer it with their case study in Beijing. They collected 30 million second-by-second vehicle activity data points on 12 vehicles, and the analysis on various sample sizes shows that over 10,000 s data points are needed for each road type and speed bin in order to limit the estimated error to below 1 %.

Besides studies with emission tests to calibrate the VSP model, other studies have attempted to improve the conventional VSP method through statistical or methodological approaches. Qu et al. [26] studied the correlation between VSP and emission under different speeds and acceleration rates. Park et al. [25] introduced a re-binning method based on vehicle speed. Based on these studies, it appears that the conventional VSP formula developed by Jiménez (1999) over 20 years ago on the basis of vehicle configurations at that time, may not be suitable for modern vehicles. Changes in vehicle emission regulations over the years have motivated car-makers to develop new technologies to meet the latest emission requirements [36,37]. The past ten years has also witnessed a gradual transition from hardware defined vehicles to software defined vehicles. Modern vehicles are now equipped with a large number of sensors, actuators, and processing Electronic Control Units (ECUs) (Bosch Professional Automotive Information, 2016). The vehicle control system employs an ECU to monitor all external and internal parameters required for vehicle operation, in order to improve emission reduction, driving experience and safety. These parameters can be read by the on-board diagnostic (OBD) interface through standard

automotive CAN-bus communication technology. Mera et al. [18] introduced a new emission modeling method named VSP + M which combined VSP with load-regime engine maps to reduce estimation errors.

The emergence and growing popularity of HEVs also poses a challenge for the traditional VSP method. The emission process of HEV is more complex due to the combined functioning of conventional internal combustion engine and electric motor [15,32,31]. The engine can be on and off during the driving. As a result, emission is not directly related to vehicle behavior. This shift in vehicle power source has led to adjustments in the conventional VSP method [40,35]. The classification and regression tree (CART) model was adopted by Zhai et al. [40] to realize the engine start and stop rules based on vehicle speed, acceleration and the product of the two for 2001 Toyota Prius HEV. Once the engine shutdown behavior is identified by the CART model, zero emission will be assigned; otherwise, the emission will be modelled following normal correlation with the conventional VSP. Holmen and Sentoff (2015) tested the 2010 Toyota Camry HEV with 118,675 s test data to verify their Percent Electric-Drive-Only (%EDO) model to statistically determine the EDO percentage at city, rural and highway conditions based on VSP. Similarly, another engine start/stop rule was proposed by Wang et al. [33] for 2020 Ford Fusion HEV with 375,840 s emission test data. This model is defined as Xtreme Gradient Boosting trees (XGBoost) model with four EOVs including VSP, road grade, vehicle speed, and acceleration. However, all these models can only help identify engine stop and electric drive mode, which is unfortunately only one application condition of a HEV. Another important activity associated with HEVs is the interaction between engine and motor, which can be taken as the engine load-shifting mode caused by battery charge and discharge. As the vehicle electrification becomes popular in recent years, Xu et al. [38] proposed a more specific approach for BEV, HEV and FCEV by a data-driven Bayesian Network statistical model. This model was applied in four HEVs with 987,092 s test datasets for each vehicle to statistically determine some key parameters including speed, acceleration, VSP, grade and battery state of charge (SOC). Owing to the introduction of SOC as an IOV parameter to improve the VSP, this model can identify-three HEV work modes: engine start/stop, hybrid and regenerative braking mode. To sum up, all the HEV models proposed so far have tried to determine the internal engine working mainly by EOVs but very limited IOV with their strong statistical data-driven approach based on many expensive and time-consuming tests.

In this study, unlike previous methods of enlarging empirical test database or improving the conventional VSP scope, a new VSP concept is introduced with the same physical meaning of conventional VSP (VSP_veh) but on the engine level, which is defined as vehicle specific engine power (VSP_eng). VSP_veh represents the power that a running vehicle on the road has to overcome; it is generally based on the externally observable variables (EOVs) such as vehicle speed, acceleration and road-grade. It does not consider the internally observable variables (IOVs) such as engine speed and intake manifold air pressure, which are considered to be more directly related to CO₂ and NO_x emissions on gasoline and diesel vehicles [33,1]. Instead of the EOVs, this study intends to estimate the engine torque output from the on-board IOVs. This involves the following processes: (1) building the semi-physical and semi-empirical torque calculation algorithm with on-board engine operating actuators and sensors in the ECU; (2) validating the algorithm accuracy on a boundary-controlled engine test bench with torque measurement covering a wide range of engine operating speed and load; (3) extending the validated ECU algorithm on a vehicle running environment where the torque is nearly impossible to be measured with an affordable equipment. Through the collaboration with the local carmakers in China, a gasoline engine was fitted on an engine test bench for the ECU algorithm development and validation processes, and then a HEV equipped with the same engine was tested following the Chinese RDE regulation on the different roads with the portable emission measurement system (PEMS), in the city of Ningbo, China. The test

results enable a direct comparison between VSP_veh and VSP_eng on their correlations with CO₂ emission, and may lead to a thorough understanding of HEV working modes.

This study aims to develop an IOV-based engine level VSP estimation method to accurately quantify the CO₂ emission of HEVs. This report was to first introduce the traditional VSP method, followed by the electronic control method of engine torque estimation using engine running IOV monitoring in ECU. An RDE test was then conducted and the test results were analyzed to demonstrate the suitability of engine level VSP as a reliable indicator for CO₂ emission. Further analyses were conducted to characterize the CO₂ emission of HEV under its different working modes. The report then ends with discussions on the application of vehicle electronics in traffic emission modeling and the potential for on-board and remote emission monitoring.

2. Materials and methods

2.1. Traditional VSP method (VSP_veh)

The traditional VSP method (VSP_veh) is based on a vehicle dynamics model of force and movement. It defines VSP_veh as the vehicle running power divided by the vehicle mass [16]. All the resistant forces applied on the vehicle are considered, essentially including the following four components: (1) the dynamics component of acceleration, (2) the gravity potential of road grade, (3) the rolling component, and (4) the aerodynamic component, as shown in Fig. 1. The first two components of VSP_veh can be described by physical expressions independent of mass, while the rolling and aerodynamic components are related to the vehicle wheel friction coefficient and car-body design, respectively. In a mathematical form, VSP_veh is expressed as Eq.1:

$$\begin{aligned} VSP_{veh} &= Power/Mass \\ &= \frac{d}{dt}(E_{Kinetic} + E_{Potential}) + (F_{Rolling} + F_{Aerodynamic}) \times v / m = \left[\frac{d}{dt} \left(\frac{1}{2} m (1 + \varepsilon) v^2 + mgh \right) + (C_R mg + \frac{1}{2} \rho_a C_D A v^2) \times v \right] / \\ &= v(a \times (1 + \varepsilon) + \times grade + g \times C_R) + \frac{1}{2} \rho_a \frac{C_D \times A}{m} v^3 \end{aligned} \quad (1)$$

where VSP_veh is the most commonly used vehicle specific power (kW/ton), $E_{Kinetic}$ and $E_{Potential}$ are the kinetic and potential energies of the vehicle (kJ), $F_{Rolling}$ and $F_{Aerodynamic}$ are the rolling and aerodynamic resistance of the vehicle (kN), v is the vehicle speed (m/s), m is the vehicle mass (ton), ε is the equivalent translational mass factor of the rotating components of the vehicle powertrain (-), g is the acceleration of gravity (9.8 m/s²), h is the altitude of the vehicle (m), C_R is the coefficient of rolling resistance (-), ρ_a is the ambient air density (kg/m³), C_D is the drag coefficient (-), A is the frontal area of the vehicle (m²), a is the acceleration (m/s²), and grade is the vertical rise divided by horizontal distance (-).

Based on Jiménez-Palacios' research (1999), the four parameters in

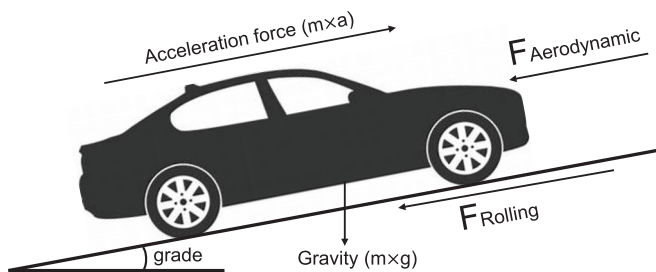


Fig. 1. Traditional VSP method considers four forces in vehicle motion dynamics.

Eq.1 (ε , C_R , ρ_a and $\frac{C_D \times A}{m}$) are further simplified as typical values based on the representative conditions. For example, the normal values of ε for a manual transmission are 0.2500, 0.1500, 0.1000, 0.0750 in the 1st, 2nd, 3rd, and 4th gear, respectively, and 0.1000 is used as a typical value for all vehicles to simplify Eq. (1). As for C_R , which depends on the road surface, and tire type and pressure, typical values range from 0.0085 to 0.0160, and a value of 0.0135 is used. Similarly, air density ρ_a is assigned a typical value of 1.207 kg/m³, corresponding to the air density at sea level under the ambient temperature of 20 °C. The fourth term, aerodynamic force coefficient $\frac{C_D \times A}{m}$, is different for each specific vehicle model and payload based on vehicle mass, vehicle type and car body design; a typical value of 0.0050 is used here for all vehicles based on an estimate of six vehicle classes as shown in Figure S1 (in Supplementary Material) with the selected vehicles presented in Table S1 for each class.

By applying these typical values to Eq.1, the simplified version of VSP_veh can be given as Eq. (2):

$$\begin{aligned} VSP_{veh} &= v(a \times (1 + \varepsilon) + g \times grade + g \times C_R) + \frac{1}{2} \rho_a \frac{C_D \times A}{m} v^3 \\ &= v(a \times (1 + 0.1) + 9.81 \times grade + 9.81 \times 0.0135) + \frac{1}{2} \times 1.207 \\ &\quad \times 0.0005 v^3 \\ &= v(1.1a + 9.81 \times grade + 0.132) + 0.000302 v^3 \end{aligned} \quad (2)$$

2.2. VSP based on engine power estimation (VSP_eng)

VSP was introduced at a time (1990s) when it was impossible to determine the engine power directly, because most engines back then were acting as a purely mechanical system with engine load adjusted directly by the acceleration pedal. Modern vehicles, however, employ advanced electronics to conduct a real-time monitoring and accurate torque control, in order to improve the driver's experience and to meet more stringent emission standards. Specifically, there are two essential factors in a torque structure control algorithm: (1) the quantitative representation of torque request from vehicle and (2) torque implementation by complex engine air-fuel-spark control [2].

Figure S2 shows a typical scheme for vehicle and engine torque control. Firstly, on the vehicle level, torque from powertrain produces tractive effort on the wheels. This is controlled by the torque structure algorithm in ECU which estimates the torque being produced and consumed by the engine operation and vehicle activity. Secondly, on the engine level, once the torque request is confirmed by the upstream torque coordinator, it is converted to a collective action for all the actuators considering the overall engine efficiency and smooth transition from previous actions.

As the torque structure algorithm is adopted to convert the vehicle control to simplified engine control, the next step is to ensure the engine can achieve the target torque output. In this study it is assumed that the torque estimation algorithm in the ECU (Figure S2) adopts a close-loop control method. The combined operation of the actuators could result in a series of engine parameter change which can be monitored by different types of sensors fitted on the engine as shown in Fig. 2 (adapted from Bosch Professional Automotive Information [2]). Here, the boost pressure and intake manifold pressure sensors are the result of turbocharge wastegate and throttle adjustment. The exhaust lambda sensor (excessive oxygen measurement) can help optimize the air/fuel ratio (AFR) to make the engine and catalytic convertor work properly. An engine speed sensor is located on the crankshaft of the engine to directly measure the rotating speed as a result of balance between propulsion torque and vehicle resistance. By monitoring these actuators and sensors, the engine torque output can be estimated by Eq. (3) based on a semi-physical and semi-empirical algorithm.

$$T_{est} = T_{ind} \times \eta_{combustion} \times \eta_{AFR} - T_{loss}$$

$$\dot{m}_a = \sqrt{\frac{T_m}{T_a}} \frac{V_d \times \eta_{vol}}{120RT_m} nP_m$$

where the variables are specified in Table S2.

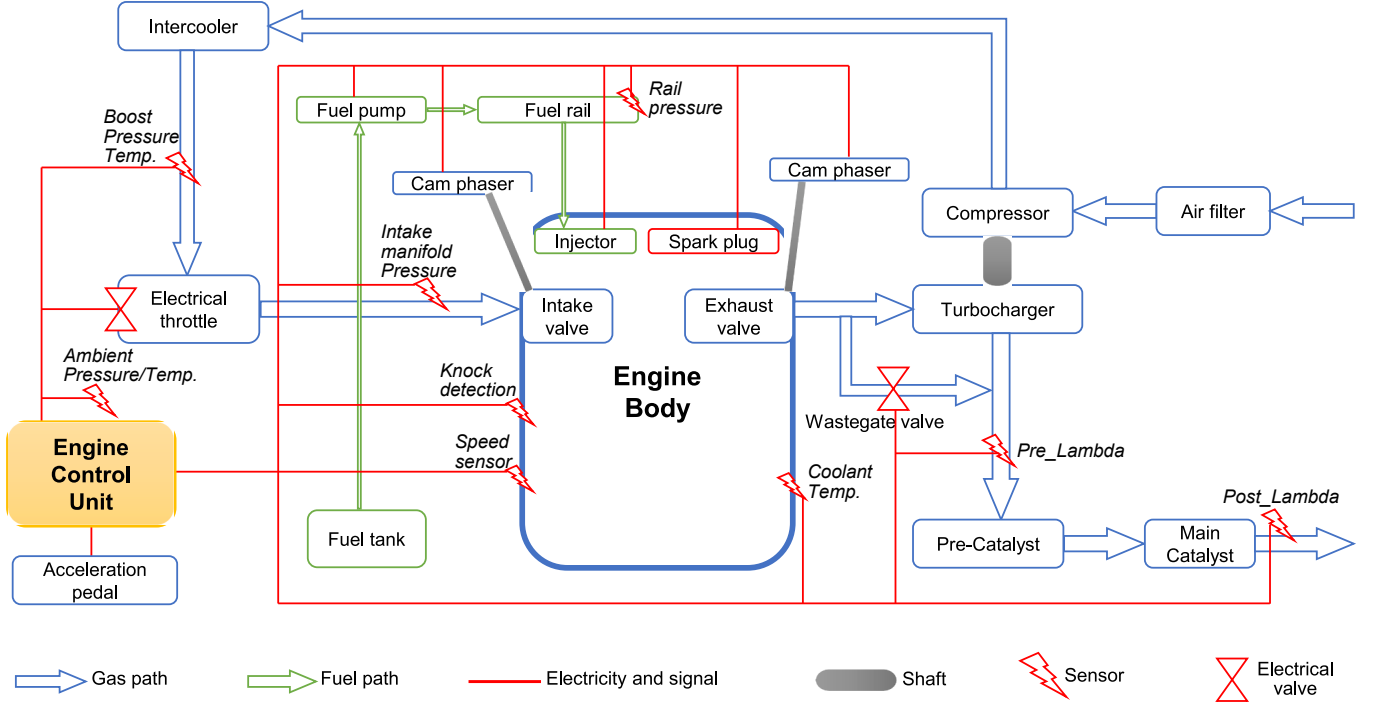


Fig. 2. Engine electronic sensors and actuators configuration for ECU.

$$T_{ind} = \frac{H_u \times \dot{m}_f \times \eta_i}{2\pi n / 60}$$

$$\dot{m}_f = \frac{\dot{m}_a}{\lambda \times L_{th}} \quad (3)$$

$$\dot{m}_a = \sqrt{\frac{T_m}{T_a}} \frac{V_d \times \eta_{vol}}{120RT_m} nP_m$$

where the variables are specified in Table S2.

As shown in Eq. (3) and Table S2, the indicated torque generation at ideal condition, T_{ind} , is calculated in three steps: (1) air path dynamics for \dot{m}_a based on ideal gas law and engine displacement filling, (2) fuel path dynamics for \dot{m}_f based on stoichiometric combustion control, and (3) energy conservation for T_{ind} based on heat-value constant of ideal combustion process. The empirical variables are natural attributes for a given engine at specific operating conditions such as engine speed and load, and engine coolant temperature; they can therefore be calibrated from laboratory engine test as illustrated in Figure S3. Here the engine is fixed on a test bench with the output flywheel connected to a torque dynamometer through a shaft to work as a load for the engine and to measure the torque. The engine is fed with the controlled air, fuel and coolant supply, and equipped with the control system in Fig. 2. By running a pre-defined sweep test under different conditions (e.g. engine speed, load, Lambda, camshaft timing, injection timing, spark timing), the test data from test bench and the ECU actuators and sensors can be merged together to calibrate the ECU algorithm with an estimated torque matched with the measured one.

Although the calibrated empirical variables are specific to a given engine from a given manufacturer, the same calibration strategy can be applied to each engine type to derive accurate values for the empirical variables. A generic calibration strategy is shown in Figure S4. Firstly, an

indicated torque is derived under ideal efficiency, based on the air mass inside the combustion chamber for different engine speeds. Then this torque can be corrected with the ignition efficiency curve which characterizes how the efficiency deteriorates with spark timing offset. Subsequently, other similar tables are adopted to calibrate for air charge, lambda efficiency, friction and pumping loss of the engine process at different engine speed, load and thermal conditions.

Results from a sample test are shown in Fig. 3. This sample is collected from 320 test points on the operating conditions with engine speed from 1,000 rpm to 6,000 rpm and engine torque from 10 Nm to 265 Nm (Fig. 3(a)). Fig. 3(b) shows the correlation between the measured torque and the estimated torque: a very good linear correlation ($R^2 = 0.9991$) is observed here. Such calibrate results are useful for generating accurate and reliable on-line torque estimation for the torque structure control system, especially for a HEV with strong torque distribution requirement between engine and motor.

Once the engine torque output is estimated and engine speed is measured, the power in a rotating mechanical system is the product of speed and torque, so the engine power based VSP can be calculated by Eq.4:

$$VSP_{eng} = Enginepower / Mass = (n_{eng} \times T_{est}) / (9550 \times m) \quad (Eq.4).$$

where VSP_{eng} is the engine level VSP (kW/ton), n_{eng} is engine speed (rpm), T_{est} is engine torque (Nm), m is vehicle mass (ton), and the constant 9550 is for unit conversion.

2.3. Vehicle test

The vehicle tested in this study is a hybrid sport utility vehicle (SUV) from a local Chinese automobile manufacturer, with its most relevant specifications shown in Table S3. The development target of this vehicle is to meet the requirements of China stage 6b emission standard to be

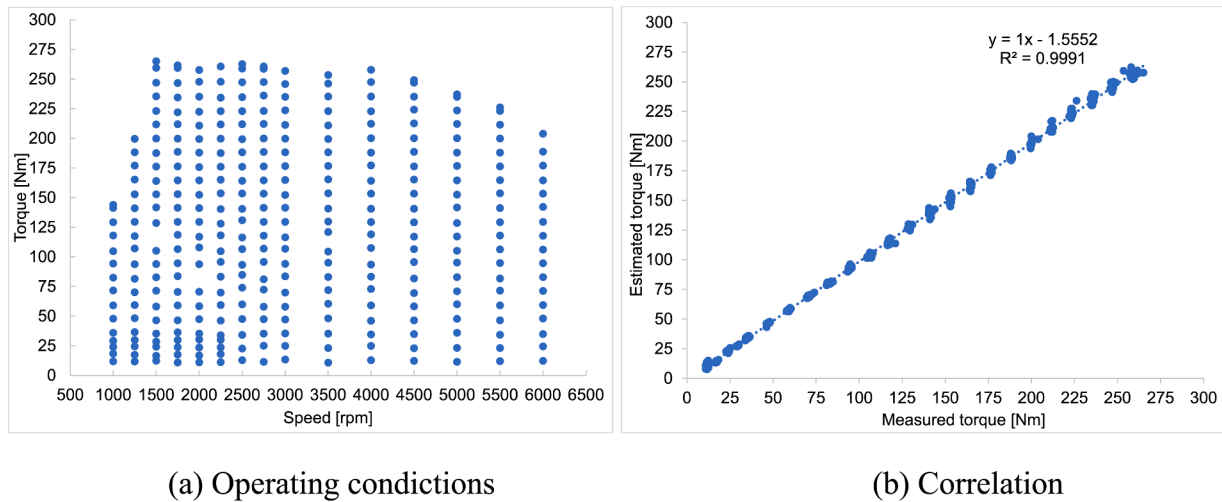


Fig. 3. Sample results of torque calibration test.

implemented in 2023, including RDE. Therefore, the exhaust from the engine after the treatment system has achieved very low-level emissions through the strict emission-oriented design and electronic control calibration. Specifically, for the hybrid architecture, this SUV is equipped with a 1.5L gasoline engine and an electric motor as shown in Figure S4. This vehicle is equipped with a dual clutch 7-speed ratio transmission which is popular for many local car makers in the Chinese market. The two clutches are matched with two sets of power transmission shafts, and all the odd gears are arranged on one shaft and the even gears plus reverse gear are placed on the other.

The RDE test was carried out on the urban, rural to highway road subsequently around the city of Ningbo in Zhejiang Province of China by following the latest China stage 6 emission regulation GB18352.6–2016 [19]. The PEMS was used to collect the gas emission concentration and exhaust mass flow, which can be applied to calculate the mass flow of CO₂ and other gas pollutants according to the technical requirement of the regulation. The PEMS used in this study is from AVL List Company (Austria) as seen in Figure S4. The on-board ECU can be directly accessed through INCA software (ETAS, Germany) by on-board diagnostic (OBD) interface, and the software can supply log file for vehicle and engine running conditions including vehicle speed, engine speed, engine torque and other sensor channels. The vehicle location and gravity information were also collected by the GPS receiver placed on the tested vehicle.

3. Results and discussion

3.1. RDE result and VSP distribution of the test in Ningbo

As required by the Chinese RDE regulation, the test was implemented on different road conditions including urban, rural and highway areas with different speed limits (60 km/h and 90 km/h). In addition, other requirements were also met including trip distance, time share on different driving conditions, and trip dynamic estimation for vehicle acceleration. The test was conducted on a pre-defined test route, which

started from the city center with a cold engine, and went through the city center for nearly 70 min as the urban driving; and then it took 22.4 mins to go through several towns near the city as the rural driving; after that the vehicle went onto national highway G15 for about 14 min as the highway driving. The total trip took 106 min to complete 91.5 km, giving an average speed of 52.0 km/h (31.4 km/h on urban road, 79.2 km/h in rural area and 110.5 km/h on highway). Summary results of the RDE test are shown in Table 1.

Fig. 4 shows the profiles of CO₂ emission, engine speed and torque, and vehicle speed during the RDE test. As for engine speed, once engine was started at the beginning, the engine maintained a high speed between 1,200 rpm and 5,400 rpm with no engine-stop for more than 800 s. Unlike the continuous running at the early stage with cold engine, there were many engine-stop activities when the vehicle drove through the rural road with the longest stop for 230 s around the middle of the cycle. The estimated torque was correlated with the measured engine speed during engine running and engine-stop periods, and the highest torque reached 215 Nm during the highway acceleration. The measured CO₂ emission was synchronized well with the engine torque operations for some steady-state running and transient spikes in the cold-engine and highway drive.

3.2. CO₂ emission rate and its correlation with VSP_{veh} and VSP_{eng}

Fig. 5 plots the CO₂ emission rates (gram per second) from the RDE test against the VSPs: VSP_{veh} in Fig. 5(a) and VSP_{eng} in Fig. 5(b). In Fig. 5(a), apart from the positive values of VSP_{veh} (in orange color), there are also many negative values (in blue color). For these negative VSP_{veh} values, positive CO₂ emission rates are still observed because the engine was still generating power even when the vehicle was decelerating. Linear regression results using positive values of VSP_{veh} (Fig. 5(a)) shows a weaker linear relationship as compared to regression using VSP_{eng} (Fig. 5(b)). This suggests that VSP_{veh} from EOVs is not a good predictor of CO₂ emission for hybrid vehicles. In contrast, a strong linear correlation is observed between VSP_{eng} and CO₂ emission rate,

Table 1
Summary results of the RDE test in Ningbo.

Item Road type	Trip duration (mins)	Duration share (%)	Trip distance (km)	Distance share (%)	Average speed (km/h)	Accumulated CO ₂ emission (g)	CO ₂ emission share (%)
Urban	69.6	65.6	36.5	39.6	31.4	6,871.2	44.0
Rural	22.4	21.1	29.6	32.1	79.2	4,290.4	27.5
Highway	14.1	13.3	26.0	28.2	110.5	4,463.6	28.6
Total cycle	106.1	100.0	92.0	100.0	52.0	15,625.2	100.0

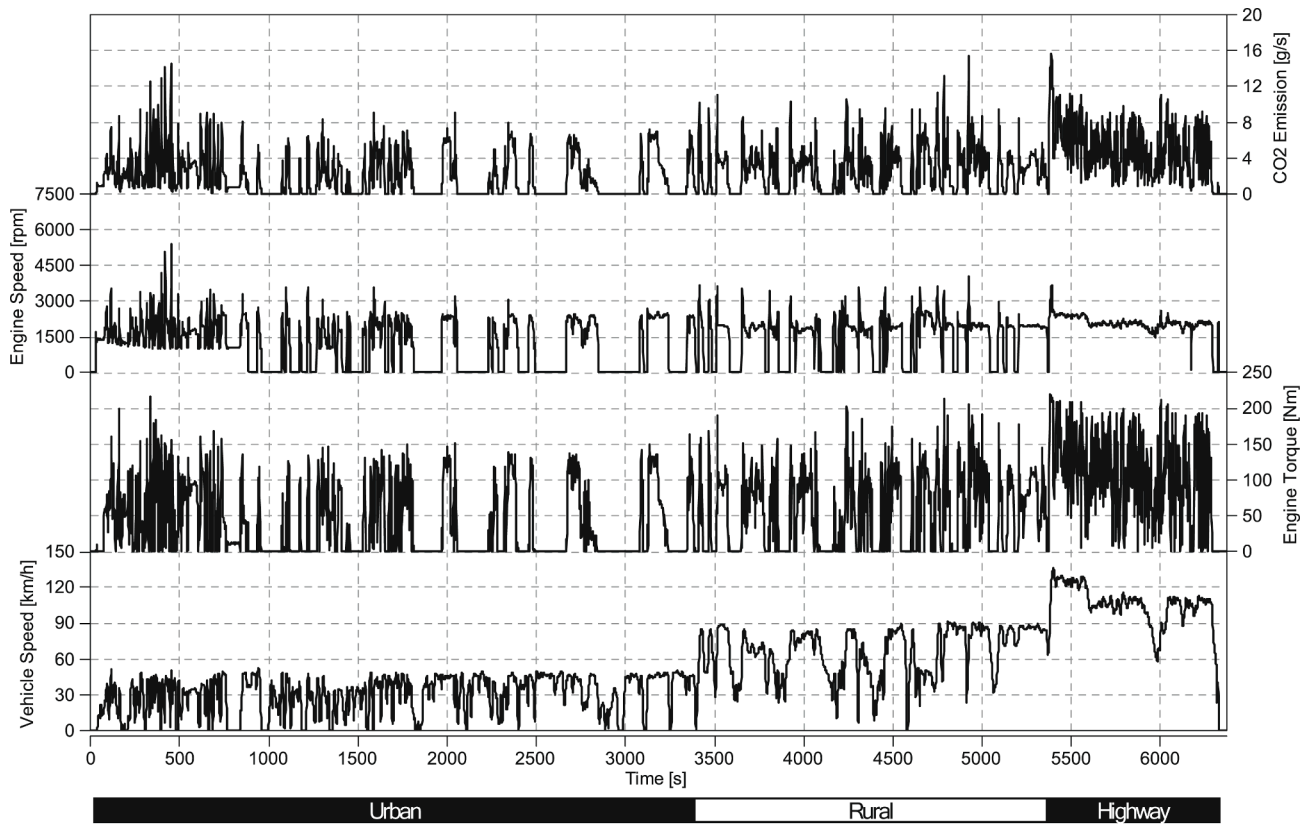


Fig. 4. Profiles of vehicle speed, engine torque, engine speed and CO₂ emission during the RDE test cycle on different types of road.

with $R^2 = 0.9783$, which indicates that VSP_eng from IOVs is a simple yet reliable predictor of CO₂ emission rate. Regardless of the hybrid working strategy, as long as the engine was in operation, the CO₂ emission rate could be directly predicted from VSP_eng using the linear regression equation with slope (0.3785) and intercept (0.1672) for this HEV (as shown in Fig. 5(b)).

To further compare the IOV-based VSP_eng and EOVB-based VSP_veh with the powertrain control strategy of the hybrid vehicle, Fig. 5(c) plots the CO₂ emission rates against the two VSPs together. Here it is interesting to see all the dots are generally distributed in four regions, each of which can be identified as representing one of the four HEV working modes: E-drive, E-boost drive, direct drive and E-charge drive.

(a) Correlation between CO₂ emission and VSP under different HEV control modes

(1) E-drive mode: this region almost overlaps with the x-axis in the VSP_veh range of 1 ~ 18 kW/ton. Here the vehicle produces positive vehicle level VSP output but close to zero CO₂ emission. This represents the pure electric driving mode of hybrid vehicle with the engine shutdown and the electric motor operating. More interestingly, no VSP higher than 20 kW/ton is recorded in this region, which likely represents the restriction from maximum battery capacity and/or motor power output for this vehicle.

(2) E-boost drive mode: in this region the engine is in operation, but the engine power seems insufficient to drive the vehicle (alternatively it might be due to the built-in mechanism to balance the optimal efficiency of the system), consequently the vehicle power request is partially provided by the motor. For example, the top right points of VSP_veh from 40 kW/ton to 56 kW/ton come from very aggressive vehicle acceleration. This sudden vehicle power demand in this hybrid vehicle could be compensated by the electric motor rather than directly from engine as the latter may cause torque built-up delay or high emission for

the intake and combustion system. As mentioned earlier regarding the restriction of battery and motor, the extra VSP compensation provided by the electric motor is around 16 kW/ton, which is still within the limit of 20 kW/ton observed in the E-drive mode area.

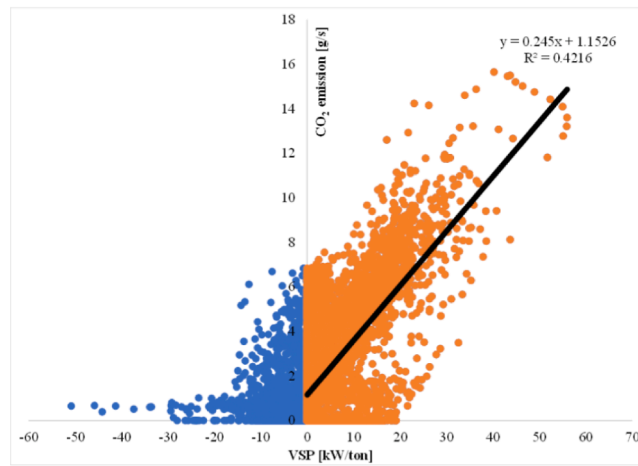
(3) Direct drive mode: in this region, the vehicle is mostly powered by the engine, without significant electrical boost from or charge for the battery.

(4) E-charge drive mode: in this region the working mode is opposite to E-boost drive. Here the power output of engine is greater than the vehicle demand, and the excessive power can be converted into electric energy by the motor and stored in the battery for the upcoming transient or pure electric driving. In this case, the engine is doing “double” jobs (both driving and charging), and the charging power is still below 20 kW/ton for the same reason as mentioned before.

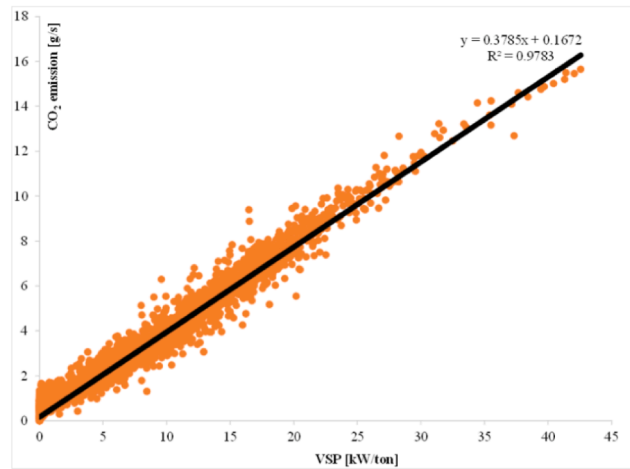
3.3. CO₂ emission rate consistency for urban, rural and highway drive tests

It should be realized that the HEV powertrain control strategy could be different when driving on urban, rural and highway roads. It is therefore meaningful to apply the same analysis as in Fig. 5(c) to different road types. The results are shown in Fig. 6. It can be seen that the correlation between VSP_veh and CO₂ emission shows very different results for different road types, while the correlation between VSP_eng and CO₂ emission remains relatively consistent: a linear relationship of slope around 0.38 and intercept close to 0 (less than 0.2 g/s) is observed for all three road types, each with a high R^2 around 0.97. Besides, when the low speeds (less than 20 km/h) are encountered on urban roads with frequent stops, the VSP_eng still has much better correlation ($R^2 = 0.95$) with CO₂ emission than the VSP_veh ($R^2 = 0.26$). This consistency indicates that VSP_eng is a reliable predictor for CO₂ emission in HEVs under various driving conditions (road, speed, etc.).

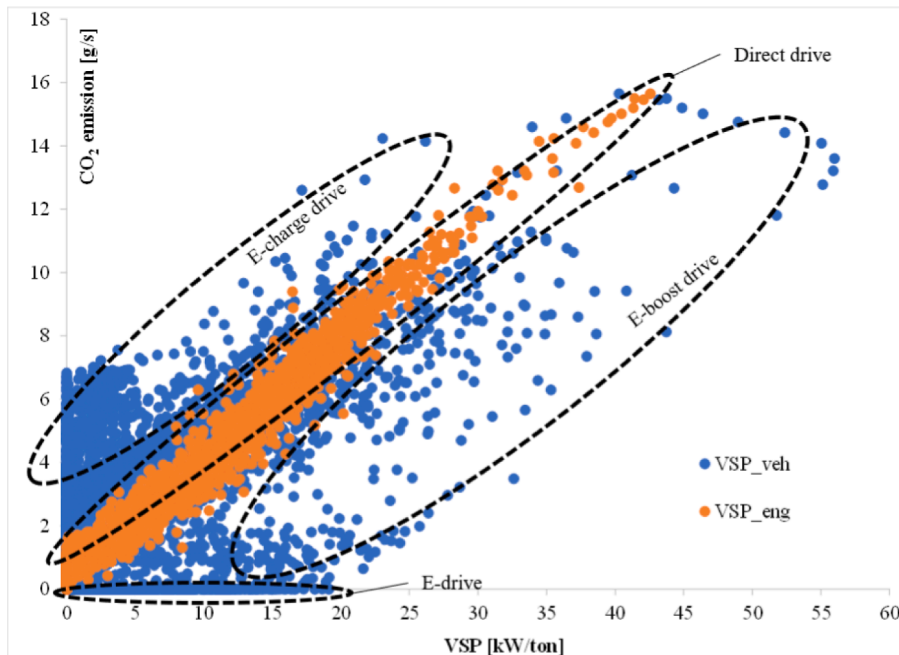
The plots in Fig. 6(a) and (b) clearly demonstrate the HEV



(a) CO₂ emission vs. VSP_veh, with regression based on positive VSP_veh only

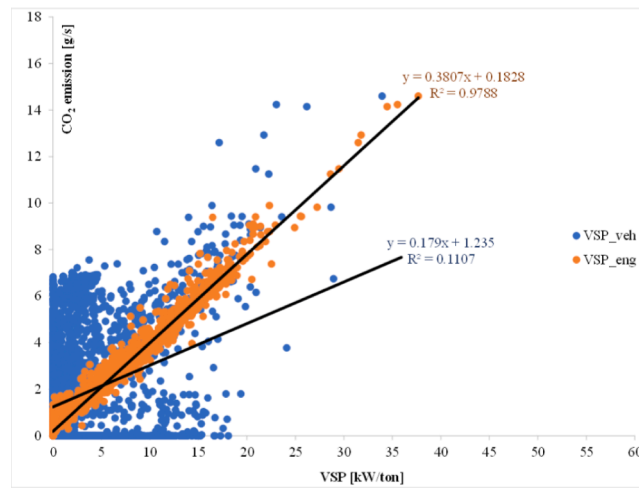


(b) CO₂ emission vs. VSP_eng

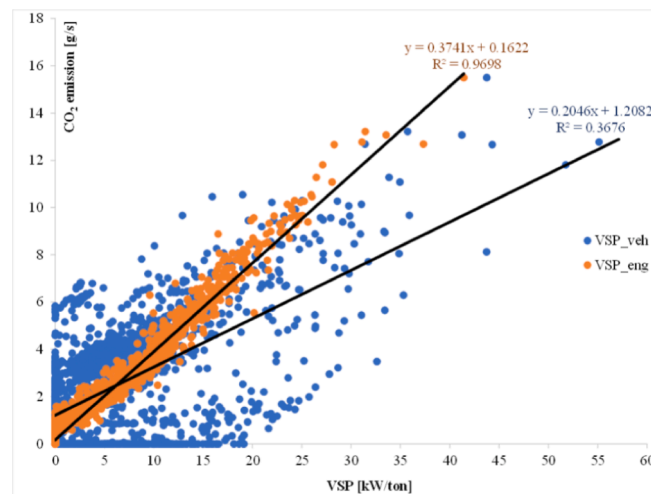


(c) Correlation between CO₂ emission and VSP under different HEV control modes

Fig. 5. Correlations of CO₂ emission rate and VSP for RDE test.



(a) Urban for all speeds



(b) Rural

Fig. 6. Correlation of CO₂ emission rates vs two VSPs under different road conditions.

characteristics with E-drive, E-boost and E-charge modes during urban and rural driving. Fig. 6(a) shows a strong presence of E-charge during urban driving, when VSP_{veh} stays below 5 kW/ton and the vehicle is powered by the engine with the battery being simultaneously charged. Besides, More E-boost occurs during rural driving (Fig. 6(b)) and on the highway (Fig. 6(c)). Fig. 6(c) further shows the absence of E-drive at high speeds; the vehicle operates under direct drive and E-boost modes for the majority of time.

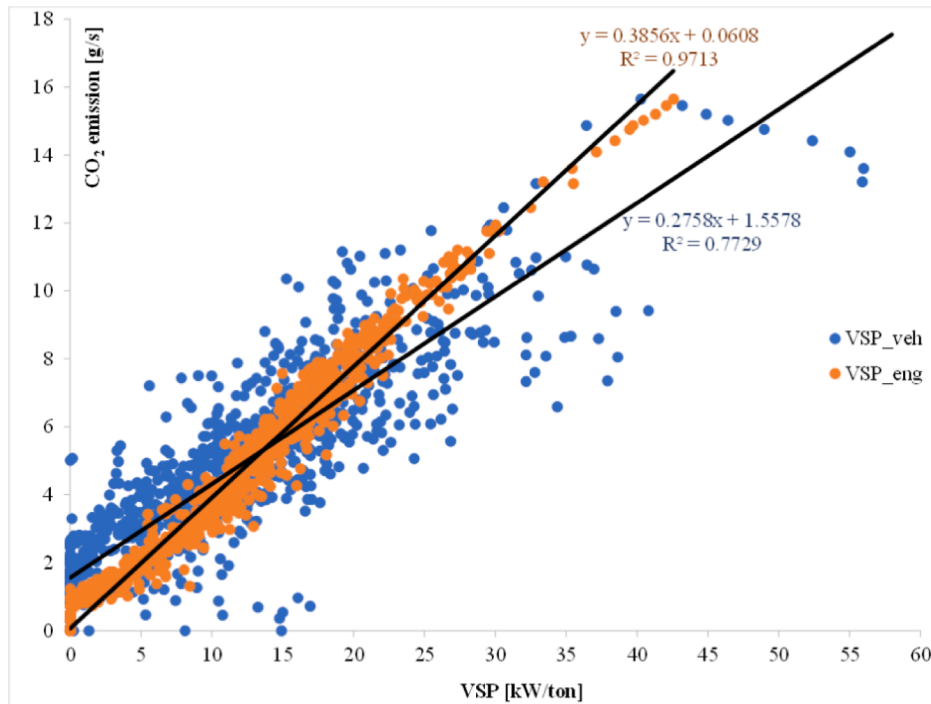
Fig. 7 shows the time frequency of different modes for each road condition, using the mode classification method illustrated in Fig. 5(c). It can be seen that the proportion of E-charge drive mode is the highest with time frequency over 45 % for all road conditions, and the proportion of direct drive mode is always the lowest. This pattern indicates a HEV control strategy where the engine, once started, runs in high power, and uses the excess energy to charge the battery. This is believed to improve system efficiency. As a result, the vehicle is less likely to run in direct drive mode. For the E-boost and E-drive modes, contrary frequencies are observed across the driving conditions: from urban to rural to highway driving, the average speed increases, and the frequency of E-boost mode also increases (from less than 9 % on the urban road to 37 % on the highway), while the frequency of E-drive mode decreases (from 43 % and 20 % in urban and rural areas, respectively, to almost 0 on the

highway).

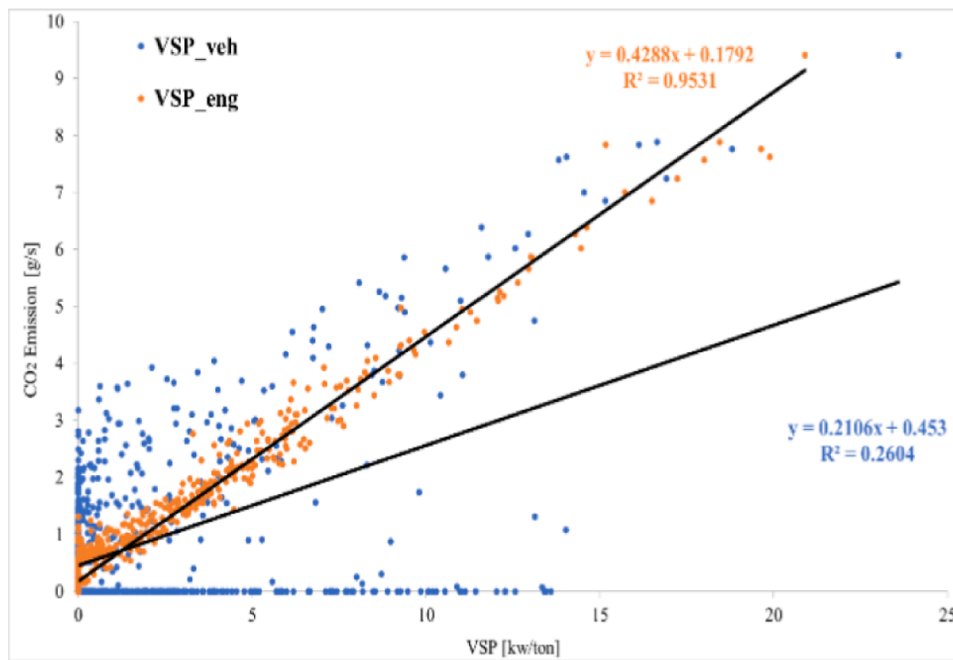
The above results also provide the evidence that both E-drive and E-boost drive modes can help reduce the CO₂ emissions. The reduction may be of various degrees and can be ascribed to two aspects: on one hand, the battery/electric motor can power auxiliary loads to decrease engine idling time when the vehicle is stopped; on the other hand, the HEV captures energy normally lost during braking by using the electric motor as a generator to store the captured energy in the battery [29].

4. Conclusions and perspective

Different from the conventional EOV-based VSP concept (VSP_{veh}), this study has developed an IOV-based VSP from the engine level (VSP_{eng}) for HEVs using an on-board engine power estimation method with the assistance of the modern electronic system equipped on the vehicle. VSP_{veh} makes it easy to estimate vehicular emission by simply considering the vehicle speed, acceleration and grade as the inputs. However, CO₂ emission is more directly linked to the combustion engine rather than the vehicle, and the macroscopic inputs acquired on the vehicle level are not sufficient to correlate the emission with the conventional VSP_{veh} for hybrid vehicles, which possess two power-suppliers (engine and battery).



(c) Highway



(d) Urban for speed lower than 20 km/h

Fig. 6. (continued).

The proposed VSP_eng method is validated by a RDE test in Ningbo city of China. Test results show that VSP_eng has a much better linear correlation with CO₂ emission rates than the conventional VSP_veh. This linear relationship is consistent on all three different roads (urban, rural and highway). The results can also be used to identify and classify four typical working modes of HEV, by plotting the CO₂ emission rates

against both VSP_veh and VSP_eng. Time frequency analysis shows that the test vehicle deploys the E-drive and E-boost drive modes for around 50 % of the time on urban road, 47 % on rural road and 36 % on the highway, demonstrating the extent of battery/electric motor being used to reduce CO₂ emission.

Although the regression results are specific to the tested HEV, the

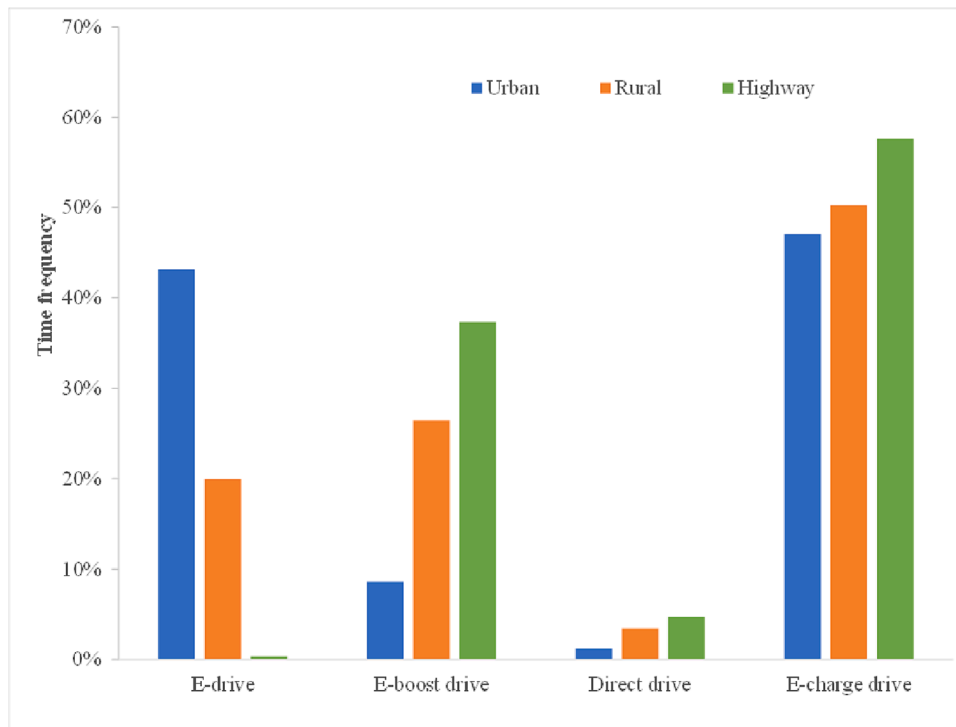


Fig. 7. Time frequency of the four working modes for urban, rural and highway driving.

same method can be applied to many other vehicles with combustion engines. The main task is to ensure the steady-state torque estimation accuracy at engine test bench. For HEVs, more tests are needed in order to verify if those four HEV working modes identified in this study are essential technical characteristics under different powertrain

configurations. Moreover, the battery charge state is another important boundary for the mode control and needs to be further investigated, especially with the rapid development in new performant batteries for HEVs. Last but not the least, it is also possible to expand the CO₂ emission prediction method to other pollutants emitted from

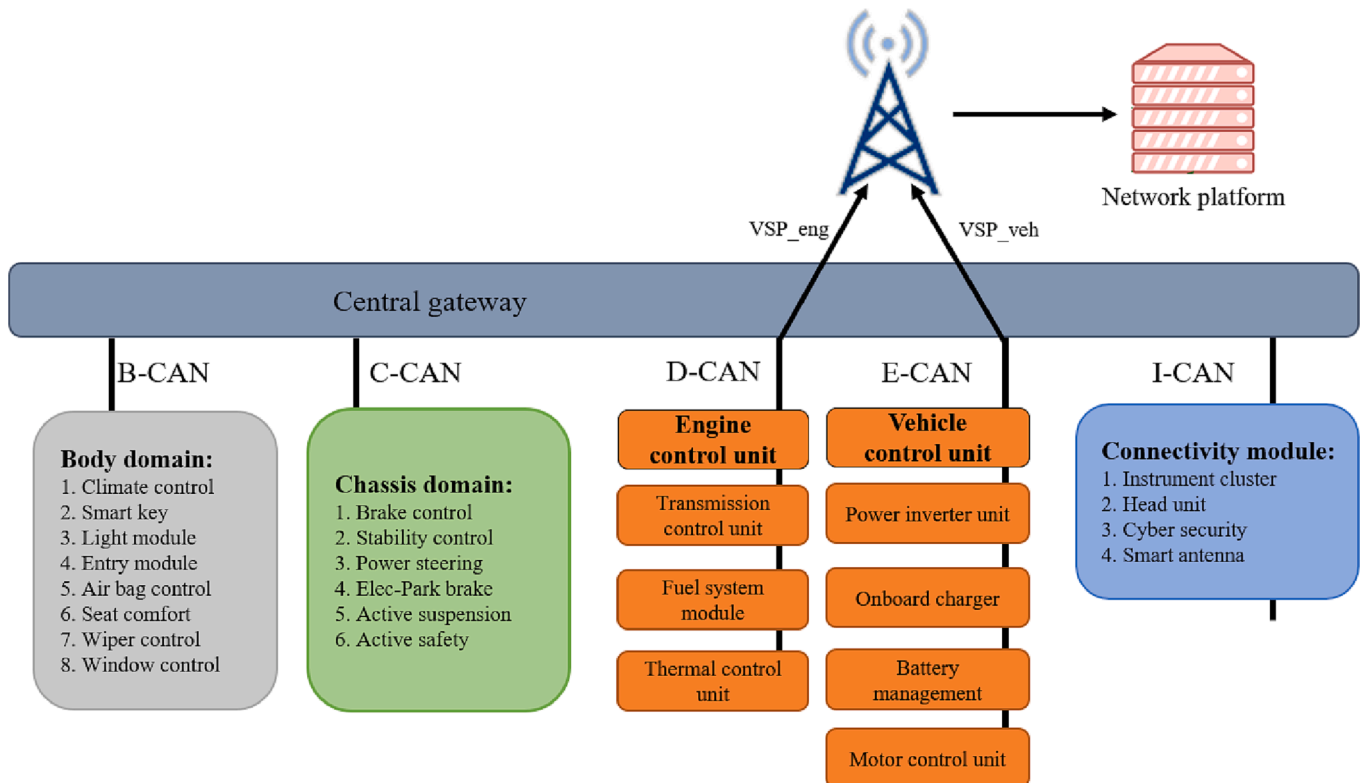


Fig. 8. VSP data exchange by next vehicle electronic architecture with V2X communication. (Adapted from [18]).

combustion engines; on one hand, the VSP_eng could replace traditional VSP as the load indicator to transfer a HEV emission to the established database in MOVEs, and on the other hand, some IOVs such as on-board air–fuel ratio could help improve the model accuracy for the emissions of CO, hydrocarbon and nitrous oxides which are very sensitive to lean or rich oxygen combustion. It should be realized that this study focuses on real time CO₂ emission estimation, and a robust evaluation of a vehicle's complete environmental carbon footprint can be based on the cradle-to-grave life cycle assessment (LCA), which will then enable the comprehensive comparison among engine-only vehicles, HEVs and electric vehicles (EVs).

As it is more representative of the vehicular engine load, the VSP_eng method appears to be a more powerful tool for emission estimation of modern vehicles. However, one critical limitation is the unavailability of estimated torque for certain vehicles: (1) vehicles without ECU, (2) vehicles with ECU but no torque structure control, (3) vehicles with torque estimation in ECU but not shared to the vehicle Controller Area Network (CAN) bus communication system. For modern vehicles, the engine speed is already a regulated channel for the OEM to send to CAN-bus according to the OBD emission regulation; if the same regulation requirement applies the torque, it will greatly enhance the real-time emission monitoring system.

Once VSP_veh and VSP_eng are quantifiable within the CAN for every single vehicle, a remote monitoring platform can be built. With 5G communication between vehicle and everything (V2X), it becomes possible to save energy and improve the HEV energy management strategy [17,39]. As shown in Fig. 8, the increased vehicle connectivity requirement will make the CAN-gateway-Ethernet-network data exchange chain more accessible to the ECU. When the electronics in vehicles are improved significantly to suit the advanced vehicular internal and external communication requirements, there will be a possibility to monitor the CO₂ emissions for the vehicles on the road by simultaneously sharing the engine and vehicle operation information such as VSP_eng and VSP_veh to the network platform, which would then pave the way for the intelligent real-time management of vehicular gas emissions on different scales.

CRediT authorship contribution statement

Wenli Wang: Investigation, Data curation, Writing – original draft, Writing – review & editing. **Jing Bie:** Investigation, Data curation, Writing – original draft, Writing – review & editing. **Abubakar Yusuf:** . **Yiqiang Liu:** . **Xiaofei Wang:** Investigation, Validation. **Chengjun Wang:** Methodology, Software. **George Zheng Chen:** . **Jianrong Li:** Writing – review & editing. **Dongsheng Ji:** . **Hang Xiao:** Formal analysis. **Yong Sun:** Supervision, Writing – review & editing. **Jun He:** Funding acquisition, Supervision, Project administration, Writing – review & editing.

Declaration of Competing Interest

The authors declare that they have no known competing financial interests or personal relationships that could have appeared to influence the work reported in this paper.

Data availability

Data will be made available on request.

Acknowledgments

This work was jointly sponsored by the Ningbo Science and Technology Innovation Key Projects (Nos. 2020Z099, 2022Z028), Li Dak Sum Fellowship from University of Nottingham Ningbo China (E06211200005) and the engagement project from Nottingham Ningbo China Beacons of Excellence Research and Innovation Institute.

Appendix A. Supplementary material

Supplementary data to this article can be found online at <https://doi.org/10.1016/j.enconman.2023.117050>.

References

- [1] Bishop JDK, Stettler MEJ, Molden N, Boies AM. Engine maps of fuel use and emissions from transient driving cycles. *Appl Energy* 2016;183:202–17.
- [2] Bosch Professional Automotive Information. Gasoline Engine Management: Systems and Components. 2015th ed, 2014: Springer Vieweg. 363.
- [3] Carrese S, Cuneo V, Nigro M, Pizzuti R, Ardito CF, Marseglia G. Optimization of downstream fuel logistics based on road infrastructure conditions and exposure to accident events. *Transp Policy* 2022;124:96–105.
- [4] Chong HS, Park Y, Kwon S, Hong Y. Analysis of real driving gaseous emissions from light-duty diesel vehicles. *Transp Res Part D: Transp Environ* 2018;65:485–99.
- [5] Duarte GO, Gonçalves GA, Baptista PC, Farias TL. Establishing bonds between vehicle certification data and real-world vehicle fuel consumption - A Vehicle Specific Power approach. *Energy Conver Manage* 2015;92:251–65.
- [6] Duarte GO, Varella RA, Gonçalves GA, Farias TL. Effect of battery state of charge on fuel use and pollutant emissions of a full hybrid electric light duty vehicle. *J Power Sources* 2014;246:377–86.
- [7] European Commission. Directorate-General for Mobility and Transport. EU transport in figures : statistical pocketbook 2020. 2020. DOI: 10.2832/491038.
- [8] European Commission. Directorate-General for Mobility and Transport. EU transport in figures : statistical pocketbook 2021. 2021. DOI: 10.2832/27610.
- [9] European Environment Agency. The first and last mile : the key to sustainable urban transport : transport and environment report 2019. 2020: Publications Office. <https://data.europa.eu/doi/10.2800/200903>.
- [10] European Environment Agency. Computer Programme to calculate Emissions from Road Transport (Version 5.6.1). 2022. <https://www.emisia.com/utilities/copert/versions/>.
- [11] European Environment Agency. Air quality in Europe 2021. 2021. <https://www.eea.europa.eu/publications/air-quality-in-europe-2021>.
- [12] Franco V, Kousoulidou M, Muntean M, Ntziachristos L, Hausberger S, Dilara P. Road vehicle emission rates development: A review. *Atmos Environ* 2013;70: 84–97.
- [13] Frey HC, Zheng XH, Hu JC. Variability in measured real-world operational energy use and emission rates of a plug-in hybrid electric vehicle. *Energies* 2020;13(5): 1140.
- [14] Fu Y, Sun W, Fan D, Zhang Z, Hao Y. An assessment of China's industrial emission characteristics using satellite observations of XCO₂, SO₂, and NO₂. *Atmospheric Pollut Res* 2022;13, no. 8.
- [15] Holmén BA, Sentoff KM. Hybrid-electric passenger car carbon dioxide and fuel consumption benefits based on real-world driving. *Environ Sci Tech* 2015;49: 10199–208.
- [16] Jiménez-Palacios José Luis. Understanding and quantifying motor vehicle emissions with vehicle specific power and TILDAS remote sensing, Department of Mechanical Engineering, Massachusetts Institute of Technology., 1999, Ph.D. <http://hdl.handle.net/1721.1/44505>.
- [17] Maul M, Becker G, Bernhard U. Service-oriented EE zone architecture key elements for new market segments. *ATZelektronik worldwide* 2018;13(1):36–41.
- [18] Mera Z, Varella R, Baptista P, Duarte G, Rosero F. Including engine data for energy and pollutants assessment into the vehicle specific power methodology. *Appl Energy* 2022;311:118690.
- [19] Ministry of Ecology and Environment PRC. Limits and measurement methods for emissions from light-duty vehicles (CHINA 6) (GB18325.6-2016). 2020. https://www.mee.gov.cn/ywqz/fgbz/bz/bzwb/dqyjbh/dqydwrrwfpbz/201612/t20161223_369476.shtml.
- [20] Ministry of Industry and Information Technology PRC. Parallel Management Regulation for Corporate Average Fuel Consumption and New Energy Vehicle Credits. 2020.
- [21] https://www.miit.gov.cn/zwgk/zcwj/flfg/art/2020/art_2337a6d7ca894c5c8e8483cf9400ecdd.html.
- [22] Ministry of Industry and Information Technology PRC. Fuel consumption limits for passenger cars. (GB19578-2021). 2021.
- [23] http://www.gov.cn/xinwen/2021-02/23/content_5588420.html.
- [24] National Development and Reform Commission (NDRC) PRC. Working Guidance for Carbon Dioxide Peaking and Carbon Neutrality in Full and Faithful Implementation of the New Development Philosophy. 2021. https://en.ndrc.gov.cn/policies/202110/t20211024_1300725.html.
- [25] Park J, Seo J, Park S. Development of vehicle emission rates based on vehicle-specific power and velocity. *Sci Total Environ* 2023;857.
- [26] Qu L, Li M, Chen D, Lu K, Jin T, Xu X. Multivariate analysis between driving condition and vehicle emission for light duty gasoline vehicles during rush hours. *Atmos Environ* 2015;110:103–10.
- [27] USEPA. Exhaust Emission Rates for Light-Duty On-road Vehicles in MOVES2014 - Final Report. 2015. <https://nepis.epa.gov/Exe/ZyPURL.cgi?Dockey=P100NNVN.TXT>.
- [28] USEPA. Population and Activity of On-road Vehicles in MOVES2014. 2016. https://cfpub.epa.gov/si/si_public_record_report.cfm?Lab=OTAQ&dirEntryId=309336.
- [29] US Department of Energy. Alternative Fuels Data Center: Fuels & Vehicles. https://afdc.energy.gov/vehicles/electric_basics_hev.html.

- [30] Vouitsis I, Ntziachristos L, Samaras C, Samaras Z. Particulate mass and number emission rates for road vehicles based on literature data and relevant gap filling methods. *Atmos Environ* 2017;168:75–89.
- [31] Robinson MK, Holmén BA. Hybrid-electric passenger car energy utilization and emissions: Relationships for real-world driving conditions that account for road grade 2020;738:139692.
- [32] Wang C, Ye ZR, Yu YB, Wei G. Estimation of bus emission models for different fuel types of buses under real conditions. *Sci Total Environ* 2018;640–641:965–72.
- [33] Wang A, Xu J, Zhang M, Zhai Z, Song G, Hatzopoulou M. Emissions and fuel consumption of a hybrid electric vehicle in real-world metropolitan traffic conditions. *Appl Energy* 2022;306:118077.
- [34] Wu B, Xuan K, Zhang X, Wu Z, Wang W, Shen X, et al. Quantitative of instantaneous BC emissions based on vehicle specific power from real-world driving diesel trucks in China. *Sci Total Environ* 2022;819.
- [35] Wu Y, Yang ZD, Lin BH, Liu H, Wang RJ, Zhou BY, et al. Energy consumption and CO₂ emission impacts of vehicle electrification in three developed regions of China. *Energy Policy* 2012;48:537–50.
- [36] Wu Y, Wang R, Zhou Y, Lin B, Fu L, He K, et al. On-road vehicle emission control in Beijing: Past, present, and future. *Environ Sci Tech* 2011;45(1):147–53.
- [37] Wu Y, Zhang S, Hao J, Liu H, Wu X, Hu J, et al. On-road vehicle emissions and their control in China: A review and outlook. *Sci Total Environ* 2017;574:332–49.
- [38] Xu X, Aziz H, Liu H, Rodgers M, Guensler R. A scalable energy modeling framework for electric vehicles in regional transportation networks. *Appl Energy* 2020;269:115095.
- [39] Ye M, Chen J, Li X, Ma K, Liu Y. Energy management strategy of a hybrid power system based on v2x vehicle speed prediction. *Sensors* 2021;21(16):5370.
- [40] Zhai H, Christopher FH, Roupail NM. Development of a modal emissions model for a hybrid electric vehicle. *Transp Res Part D: Transp Environ* 2011;16(6):444–50.
- [41] Zhai Z, Song G, Yu L. How much vehicle activity data is needed to develop robust vehicle specific power distributions for emission estimates? A case study in Beijing. *Transp Res Part D: Transp Environ* 2018;65:540–50.
- [42] Zhou G, Chung W, Zhang X. A study of carbon dioxide emissions performance of China's transport sector. *Energy* 2013;50(1):302–14.